Evanescent Lamb waves in viscoelastic phononic metastrip

Wei Guo,[1] Shu-Yan Zhang,[2] Yan-Feng Wang,[1,*] Vincent Laude,[3] and Yue-Sheng Wang[1,2]

[1]*School of Mechanical Engineering, Tianjin University, 300350 Tianjin, China*
[2]*Institute of Engineering Mechanics, Beijing Jiaotong University, Beijing 100044, China*
[3]*Institut FEMTO-ST, CNRS, Université Bourgogne Franche-Comté, Besançon 25030, France*

In this paper, the propagation of evanescent Lamb waves in the one-dimensional viscoelastic phononic metastrip is studied. The metastrips are fabricated by either steel or epoxy. For different metastrips, complex band structures and transmission spectra of Lamb waves are calculated by the finite element method. Furthermore, different slicing forms are also discussed. In this paper, the numerical simulations including K-V model are consistent with the experimental results. We use the exponential decay curve to quantitatively characterize the attenuation of the evanescent wave inside the band gap, and we successfully used the complex band structure to predict the displacement distribution curves in the simulation. The epoxy metastrip has smoother band-gap bounds and transmission spectrum. The effect of different slicing forms leads to changes in the complex band structure and the transmission dips occur. The present work lays the foundation for the study of common viscoelastic materials in real life.

I. INTRODUCTION

Phononic crystals (PCs) are composed of materials with different properties and arranged periodically in the spatial space[1]. The most striking feature of PCs is the band gap, inside which the wave propagation will be prohibited[2]. This feature has led to a range of applications, such as acoustic insulation[3], and filters[4]. According to the real band structure, bandgap appears when there are no dispersion curves for a particular frequency range. However, according to the energy conservation, the wave cannot disappear inside a bandgap. Then, how do waves exist? Actually, it is evanescent wave that exists in the bandgap, which should be characterized by using complex band structures[5]. The relationship between the real part of the wave number and the frequency in the complex band structure is the dispersion, and the relationship between the imaginary part and the frequency characterizes the attenuation characteristics[6].

In addition to evanescent bulk waves[7–9], complex band structures are also widely used for studying evanescent Lamb waves. Some of the investigations are only focusing on flexural waves. Han et al calculated complex band structure of phononic Euler beam by modifying the transfer matrix method[10], where the state parameters in the transfer matrix method is replaced by the initial parameters. Liu and Hussein investigated the flexural wave propagation in periodic Timoshenko beams[11]. Effects of the various types and properties of periodicity on the complex band structures are discussed. Airoldi and Ruzzene designed a tunable one-dimensional metamaterial beam using periodic shunted piezoelectric patches[12]. They showed that a comprise in the resistance should be struck between the bandwidth and attenuation, determined by the minimum imaginary part of wave number. Meanwhile, there are also studies focusing on the full types of Lamb waves. Oudich and Assouar calculated complex band structures of two-dimensional phononic plate by using the extended plane wave expansion method[13]. Effects of the plate thickness on the evanescent waves,including their polarizations are discussed. Gao et al investigated evanescent waves propagation in periodic nested acoustic black hole structure. Different attenuations of flexural and longitudinal waves are characterized by the complex band structures and verified experimentally[14].

In practice, the solid components are not ideally elastic. Viscosity might exist in some extent, especially for polymers[15]. According to the viscoelastic model, the existing studies can be classified into two types. The first is the generalized Maxwell model. The generalized Maxwell model consists of several spring-dampers in parallel to form and it takes into account the relaxation time of the viscoelastic materials. Li et al show the complex viscoelastic properties of three-dimensional metamaterials and the effect of thickness and shape of the hole on the attenuation of Bloch waves is revealed.[16]. Yi et al described the mechanical response of a viscoelastic metamaterial composed of epoxy resin and rubber. They found that by adjusting the mass of the two oscillators in the cell, a quasi-bandgap is created, which results in a wider isolation bandwidth.[17]. Lewińska et al studied a locally resonant acoustic metamaterial consisting of tungsten, epoxy and rubber and found that the viscoelastic material affects both the band gap location and also the attenuation of waves at frequencies around the band gap[18]. Then we focus on the Kelvin-Voigt viscoelastic models, where a frequency-dependent loss is equivalently added to the imaginary part of the modulus. Collet et al calculated a two-dimensional complex band structure of a plate and used the minimum value of the ratio of the imaginary part of the wave number to the amplitude of the wave number at the same frequency to estimate the attenuation of evanescent waves in the band gap[19]. Krushynska et al used the K-V model and the generalized Maxwell model to calculate dissipative solid acoustic metamaterials consisting of rubber. By comparing these two viscoelastic models it can be found that the Kelvin-Voigt model provides reliable results at medium to high frequencies[20]. Lou et al investigated the longitudinal wave propagation in the viscoelastic compos-

ite rod. Coupling of viscosity of the host material and the damping of the resonator are helpful to widen the band gap and enhance wave attenuation[21]. Krushynska et al compared elastic model, K-V model and generalized Maxwell model to predict the experimentally measured viscoelastic curves, this reveals the correlation between the viscous effect of the plate and the transmission spectrum was measured experimentally[22]. The above work has further investigated the application of viscoelastic models to viscoelastic materials. However, these articles rarely combine the complex band structure and transmission spectrum of viscoelastic materials to analyze the propagation of evanescent waves in the plate. And few experiments were conducted.

In this paper, we focus on the propagation of evanescent waves in the viscoelastic metastrips cut from an epoxy slab perforated with periodic rectangular holes. Complex band structures and transmission spectra of the metastrips are calculated using the finite element method. Viscoelasticity is introduced by considering the Kelvin-Voigt model. Displacement distributions of evanescent waves are imaged by using a vibrometer. A theoretical model is developed that predicts accurately the displacement distribution in the transmission modes. Effects of the slicing forms on the complex band structures are discussed. For comparison, metastrips cut from a lossless steel slab are also investigated. It is found that the experimental transmission of the viscoelastic metatrip can be precisely evaluated when the K-V model is involved in the simulation. The spatial attenuation of evanescent waves can be characterized by the lowest two orders of imaginary wave number. Different slicing forms can result in the reconstruction of evanescent waves, leading to the appearance or close of Bragg gap or avoided-crossings.

II. NUMERICAL AND EXPERIMENTAL METHODS

For harmonic wave propagation in the elastic solid, the dynamic equilibrium equation is:

$$\rho\omega^2\mathbf{u}(\mathbf{r}) + \nabla\cdot\mathbf{C}:\nabla^s\mathbf{u}(\mathbf{r}) = \mathbf{0}, \tag{1}$$

where ρ is the mass density, ω is the angular frequency, $\mathbf{C}$ is the elastic Hook tensor. $\nabla^s\mathbf{u}(\mathbf{r}) = 1/2(\nabla\mathbf{u}(\mathbf{r}) + (\nabla\mathbf{u}(\mathbf{r}))^T)$. According to Bloch theorem, the displacement has the following form[23]:

$$\mathbf{u}(\mathbf{r}) = \mathbf{u}_n(\mathbf{r},\mathbf{k})e^{-\imath\mathbf{kr}}, \tag{2}$$

where $\mathbf{r} = (x, y, z)$ is the coordinate vector and $\mathbf{k} = (k_x, k_y, k_z)$ is the wave vector, $\mathbf{u}_n(\mathbf{r},\mathbf{k})$ is a periodic function of coordinate. For one-dimensional periodic structures, we have $\mathbf{k} = (k_x, 0, 0)$. To get the complex band structure, the wave number should be involved in the governing equation. This could be obtained by substituting

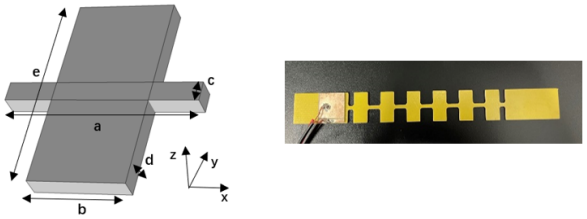

(a) (b)

Figure 1: Structure of the unit cell and the metastrip. (a) The unit cell. (b) The metastrip of epoxy.

Eq. (2) into Eq. (1), and we can obtain a generalized eigenvalue equation:

$$\begin{aligned}\rho\omega^2\mathbf{u}_n(\mathbf{r}) + \nabla\cdot\mathbf{C}:\nabla^s\mathbf{u}_n(\mathbf{r}) - \imath\mathbf{C}:\nabla^s\mathbf{u}_n(\mathbf{r})\cdot\mathbf{k}\\ -\imath\nabla\cdot\mathbf{C}:\frac{1}{2}\left[\mathbf{u}_n(\mathbf{r})\otimes\mathbf{k}+\mathbf{k}\otimes\mathbf{u}_n(\mathbf{r})\right]\\ +\mathbf{C}:\frac{1}{2}\left[\mathbf{u}_n(\mathbf{r})\otimes\mathbf{k}+\mathbf{k}\otimes\mathbf{u}_n(\mathbf{r})\right] = \mathbf{0},\end{aligned} \tag{3}$$

In this paper, we use the partial differential equation (PDE) module of finite element software COMSOL to calculate the complex band structure. First we focus on the H-type metastrip shown in Fig. 1. The periodicity is a=20 mm. Other geometric parameters of the unit cell are b/a=0.5, c/a=0.1, d/a=0.1, and e/a=1. Periodic boundary condition is applied on the surfaces perpendicular to the x-axis direction, and the other surfaces are set as free. The CBS can be obtained by choosing the eigenvalue as $\Lambda = -\imath k$ and sweeping the frequency of interest.

Meanwhile, experimental measurements are carried out to investigate the propagation of evanescent waves. Asymmetric wave source is applied on the left of the metastrip by attaching a piezoelectric patch on the strip in Fig. 1(b). The responses are collected on the right part of the metastrip by using the Polytec scanning vibrometer. Detailed experimental process can be refered in Ref.[24]. For comparison, we also calculate the transmission spectrum of a three-dimensional finite metastrip by applying an out-of-plane excitation. As a comparison, we calculated the steel material for the same structure and the results are shown in Appendix.

III. EVANESCENT WAVE IN THE EPOXY METASTRIP

As a kind of polymer, the viscosity of epoxy is generally more pronounced compared to the common solid (e.g. steel), making it more difficult to predict its wave behaviors with an elastic model. Therefore, we introduce the K-V model to characterize the viscoelastic behaviour of epoxy. In general, the K-V model has the following

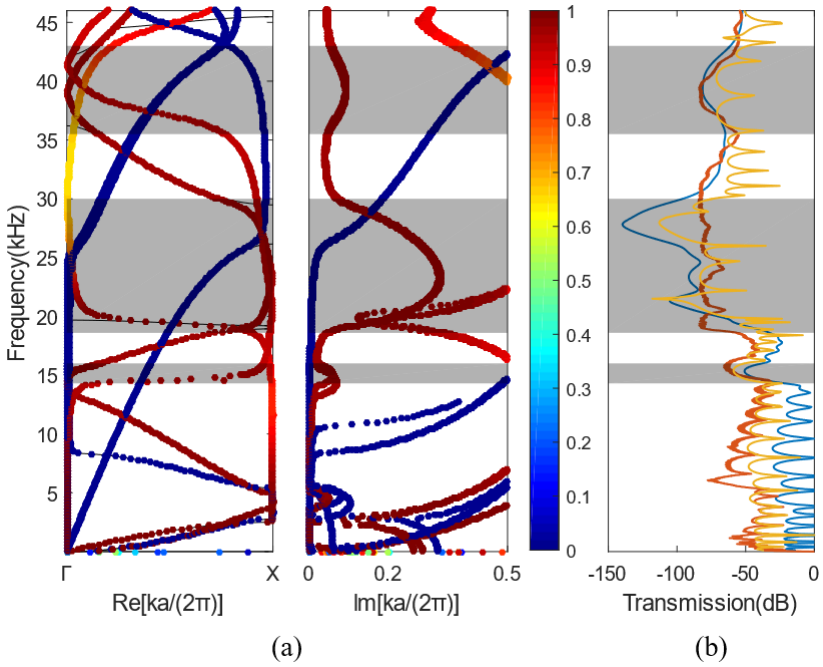

Figure 2: Complex band structure (a) and transmission spectrum (b) of the epoxy metastrip. The left and right panels in (a) show the variation of frequency with the real and imaginary wavenumbers respectively. The colorscale indicates the polarization of waves from in-plane modes (blue) to out-of-plane mode (red). The black solid line is the real band structure of the elastic model. The grey area represents the band gap. Regarding the transmission spectrum, the red line represents the experimental result. The blue and yellow lines represent the numerical results based on the K-V model and elastic model respectively.

form:

$$E = E^{'} + \imath\omega\eta, \tag{4}$$

where the Young's modulus E consists of both real part E and imaginary part. The imaginary paft of modulus is frequency-dependent with η being the viscous coefficient. The material parameters used for epoxy are $E = 2.4 \times 10^{10} + \imath 6 \times 10^{3}\omega$ Pa, Possion's ratio $\nu = 0.41$ and mass density $\rho = 2037.67$ kg/m^3. The K-V model is reduced to the elastic model when the viscosity is neglected.

A. Complex band structure and transmission spectrum

Complex band structure and the transmission spectrum of the epoxy metastrip involving K-V model are shown in Fig. 2. To distinguish different polarized modes, we further calculate the polarization amount p_w of out-of-plane waves:

$$p_w = \frac{\int_s |w|^2 dS}{\int_s (|u|^2 + |v|^2 + |w|^2) dS}, \tag{5}$$

where (u, v, w) are the three components of displacement vector (u). The elastic model is additionally calculated for comparison. As shown in Fig. 2(a), the results of the complex band structure calculated by K-V model change significantly compare to the elastic model, and in the real part of the complex band structure, a smooth band structure appears at frequencies near the high symmetry point. As the frequency increases, the effect becomes more obvious. Comparing the transmission spectrum, a clear attenuation phenomenon can be observed within the band gap of the shaded region as shown in Fig. 2(b). The steel results are shown in Fig. 8 in the Appendix. The red line represents the experimental result, the blue line and yellow line represent the result of the K-V model and elastic model of FEM respectively. Both the K-V model and the elastic model are consistent with the experimental transmission spectrum well at low frequencies 14.3-16 kHz and 18.6-30.1 kHz, but only the K-V model consistent with the transmission spectrum better in the high frequency range 35.5-43.2 kHz. It can be found that the transmission curves are smoother with the addition of the viscosity term, and it can be clearly observed that the results obtained from the K-V model are more consistent with the experimental curves. Compared to the curves in Fig. 2 and Fig. 8 it can be seen that there are similarities and differences in the overall trend. The epoxy metastrip include smoother band gap boundaries and less wavy curves. Since the structure of the metastrip is the same, these differences can only be attributed to the viscoelastic nature of the epoxy.

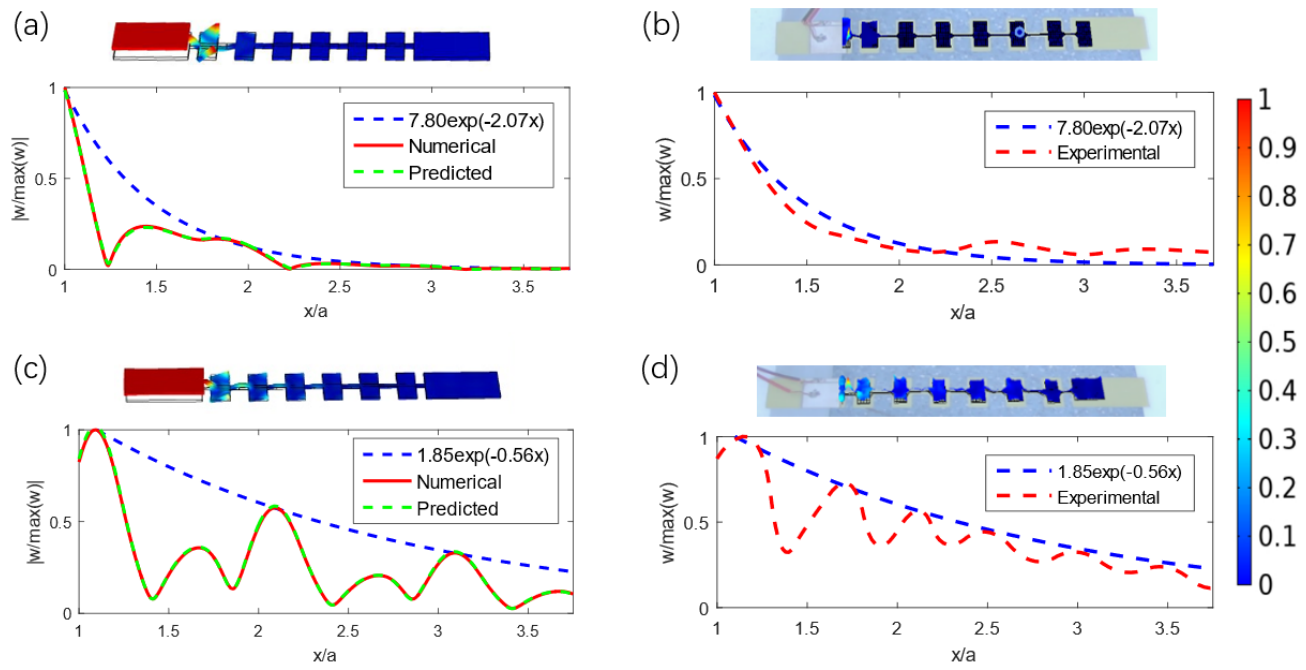

Figure 3: Attenuation of evanescent waves in epoxy metastrip. Panels (a) and (b) show the displacement distribution of the metastrip at 24 kHz obtained from simulations and experiment, respectively. The colorscale represents the amplitude of normalized displacement. Numerical displacement distribution along the central line of the top surface is shown in solid line in the bottom part of panel (a). Measured displacement distribution along the central line of the top surface is shown in solid line in the bottom part of panel (b). The predicted results are shown by green dashed lines where $\alpha = 0.66$, $k_1 = -2.03 + 3.11i$, $\beta = 0.33$, $k_2 = -2.06 - 9.46i$. The bule dashed line represents the exponential-like decay of the measured displacement fitted by the minimu imaginary part of the wave number in the complex band structure. Panels (c) and (d) show the similar results at 40 kHz. Where the coefficients in the prediction curve $\alpha = 0.5$, $k_1 = -0.55 - 0.07i$, $\beta = 0.5$, $k_2 = -0.56 - 6.35i$.

B. Attenuation of evanescent wave

The fields of the epoxy metastrip at 24 kHz and 40 kHz were obtained experimentally, as shown in Fig. 3 (The steel results are shown in Fig. 9 in the Appendix). Similarly, it can be learned that the attenuation is smaller at 40 kHz and larger at 24 kHz, which can be clearly shown in the fields.

To quantitatively characterize the attenuation of the evanescent wave inside the band gap, the images of the displacement according to the change of coordinates are given. The imaginary part has a parabolic variation and has a maximum at the central frequency as shown in Fig. 2(a). According to Bloch's theorem, there is an exponential decay along the wave propagation direction inside the structure[25–27]. To demonstrate this phenomenon, we select two frequency points (24kHz and 40kHz) and plot the displacement distribution curves at the top surface of the structure[25], as shown in Fig. 3. We measured the displacement at the centerline of the metastrip by simulation and experiment, and we use the modes of the complex band structure to predict the curves obtained from the simulation. At the same frequency of the complex band structure, there exist many modes. The prediction curve has the following form:[28]

$$w(x,y) = \sum_{n=1}^{m} \alpha_n w_n(x,y) e^{ik_n x}, \tag{6}$$

where w_n represent the displacement fields extracted from the modes, respectively. k_n represent the complex wave vectors corresponding to the modes. α_n are the coefficients. Here, we perform the calculation of the prediction curve using the two lowest modes. The expression has the following form:

$$w(x,y) = \alpha w_1(x,y) e^{ik_1 x} + \beta w_2(x,y) e^{ik_2 x}. \tag{7}$$

The red lines in Figs. 3. (a) and (b) represent the displacement distribution curve obtained from simulation and experiment at 24 kHz. The green dashed line represent the predicted curve by using complex structure.The modes of the complex band structure are found at the corresponding frequencies and their displacement fields are extracted and multiplied by the coefficients of decay, and finally their prediction curves are obtained. The blue dashed line indicates the displacement distribution curve,

where a is the values obtained by fitting the curve. Similarly, Fig. 3(c) and (d) represent the displacement distribution curve for simulation and experiment at 40 kHz, respectively. Both of simulation and experimental results are within the error tolerance. By comparing the graphs in Fig. 3 horizontally and vertically, the results of the exponential values of the decay curves obtained from simulation and experiment are similar with the same decay trend at the same frequency. The simulated numerical curves largely coincide with the predicted curves and the feasibility of fitting the numerical curve using the modes of the complex band structure is demonstrated. For the attenuation curves at different frequencies, the attenuation trends are different. This is related to the degree of attenuation of the evanescent wave, the minimum imaginary value of the complex band structure. It can be found that with the increase of the minimum imaginary part, the decay effect of the curve is different. Based on the viscoelasticity of epoxy metastrip and the K-V model, a closer fitted curve can be obtained, indicating that the K-V model can predict the viscoelastic behavior of epoxy metastrip.

By comparison, it is found that due to the viscoelasticity of the epoxy metastrip and the elastic of the steel(The results for steel are shown in the appendix), the coupling between the propagation and evanescent modes caused by the loss can be clearly found in the complex band structure due to the more involute tendency of the solid part of the epoxy resin metastrip near the high symmetry point compared to the elastic case, which leads to a more circular band gap boundary.

IV. I-TYPE OF THE METASTRIP

Next, we study the effects of different cutting methods and structures on the wave characteristic. In this work, we consider two cutting methods, as shown in Fig. 4. The models for Fig. 4(a) yellow and blue shaded areas called H-type (as discussed in section III) and I-type, respectively. The different cutting methods lead to a different structure of the individual cell connections, which has an impact on the band structure and transmission spectrum[29]. Therefore, we now further calculated the complex band structure and transmission spectrum of the I-type metastrip. The metastrips used in the experiment are shown in Fig. 4(b).

The complex band structure of the I-type epoxy metastrip is shown in Fig. 5(The steel results are shown in Figure 10 in the Appendix). The shaded areas are the band gap. It is obvious that the I-type leads to the appearance of more wave modes. As shown in Fig. 5(a) point A, a mode in the torsional direction can be clearly observed. Since the direction of the periodic boundary is the same as that of wave propagation, and the appearance of the model shown in the figure indicates that it is a non-excitable mode. It is called the deaf band[27] which cannot be excited. This is related to the symmetric form of the mode corresponding to the excited state of the source, and therefore they cannot transmit acoustic energy in the PCs. In the deaf band range, even with out-of-plane wave propagation, a directional band gap can still be generated. The mode at point B is an in-plane mode, rotating at a central point. Though its band runs through the entire frequency range, it does not affect band gap. However, as can be seen in Fig. 5(b), there are many sharp vibrations in the transmission spectrum compared to the H-type. This is due to the cutting method which leads to a narrow width of the beam structure on both sides and the force of the beam. The transmission spectrum obtained by the K-V model is closer to the experimental result compared to the elastic model. Especially in the high frequency region, the amplitude of the K-V model is closer to the experimental value. This indicates that the K-V model can better predict the transmission spectrum of the viscoelastic model.

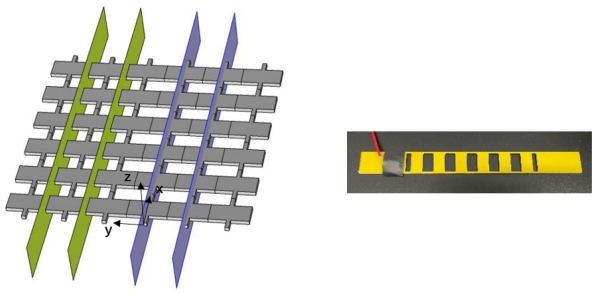

(a) (b)

Figure 4: Schematic diagram of H-type and I-type and the metastrip in the experiment. (a) The yellow and blue cut areas indicate the H-type and I-type, respectively. The coordinate system is established in the position shown in the figure, at this time y = 0. (b) The metastrip of epoxy.

V. THE EFFECT OF DIFFERENT SLICE POSITIONS ON THE COMPLEX BAND STRUCTURE

We explore the complex band structure and transmission spectrum of the I-type metastrip in IV, and here we further investigate the effect of different slicing distances on the complex band structure. In this section we use the elasticity model of the epoxy to do the simulation work to calculate the complex band structure and to investigate the effect of different slice distances on the complex band structure.

As shown in Fig. 4(b), the yellow shaded region of the I-type structure is cut by translating it along the y-axis direction. Define the initial displacement of I-type as y=0. We calculated the complex band structure at different positions and the results are shown in Fig. 9. When y=10 mm, which is what we previously described as the

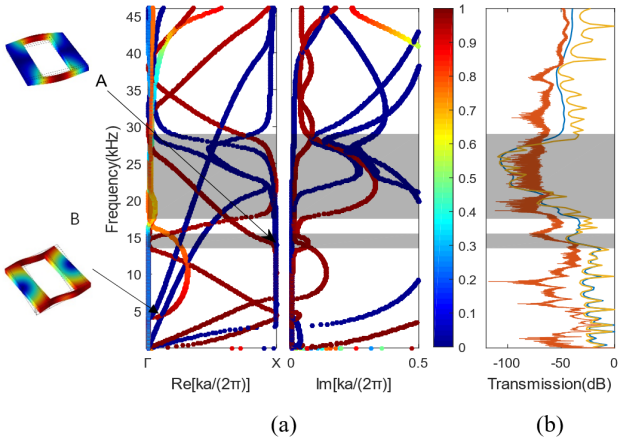

Figure 5: The complex band structure and transmission spectrum for the epoxy metastrip. (a) The complex band structure for the I-type epoxy metastrip and the modal distruibutions at marked points A and B. The left and right plots show the frequency variation with the real and imaginary wave number, respectively. The grey regions represent the band gaps. Panel (b) shows the transmission spectrum. The red line represents the experimental result, the blue and yellow lines represent the K-V model and elastic model of FEM.

H-shaped structure as a comparison. It can be observed that the three band gaps in frequency range 14.3-16 kHz, 18.6-30.1 kHz, 35.5-43.2 kHz gradually appear with the increase of slicing distance. The deaf band disappears as in Fig. 4(a). For the band of the in-plane mode C in Figs. 7(a)-(e), the complex band structure coincides with the band structure, which indicates the traveling wave. For point D in Fig. 7 (c)-(f), this band represents an evanescent wave. The initial frequency increases gradually and the frequency range increases as y increases. Viewing the bands corresponding to the avoid crossing of point E in Fig. 7(f). The avoid crossing appear in Fig. 7(a)-(e), which is a phenomenon of non-crossing of bands due to the mutual coupling between different modes. The two modes are interchanged around the intersection and this coupling appears weaker as the slice distance increases[30]. By observing Fig. 7(a)-(e), it can be found that the band gaps located at 14.3-16 kHz and 35.5-43.2 kHz gradually appear. For the band at point F in Fig. 9, it can be observed that as y increases, the slope of its tangent line increases and then decreases and finally becomes negative. This change is easier for the generation of low frequency band gap and the band gap of the lowest level bending wave becomes narrower and then wider. As the slicing distance increases, it is found that the value of minimum imaginary part gradually becomes smaller. On the contrary at 18.6-30.1 kHz, the value of minimum imaginary part first decreases and then increases, reaching a maximum when y=10 mm. In summary, the slicing method has less effect on the out-of-plane mode and more on the in-plane mode.

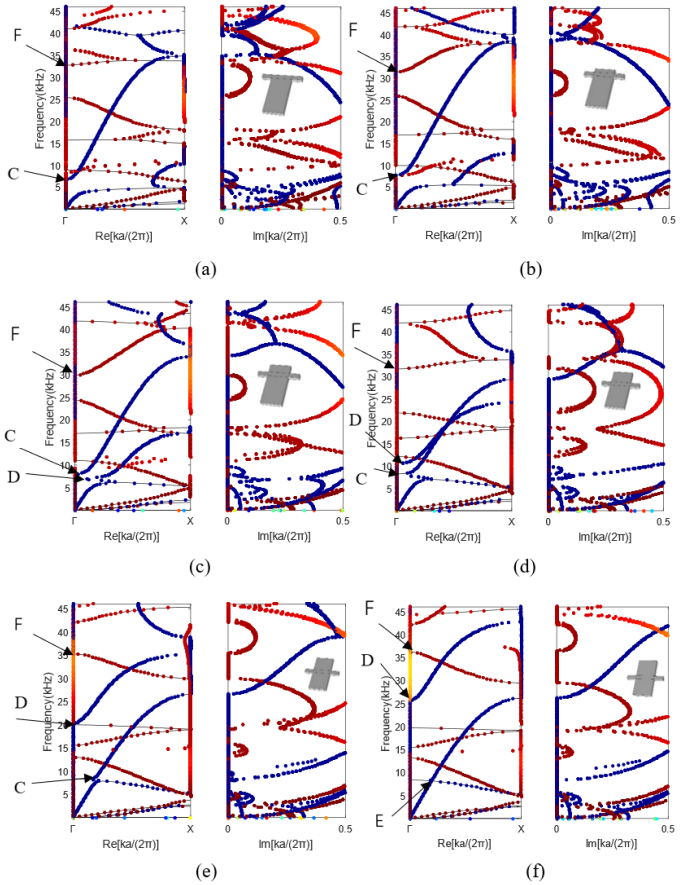

Figure 6: Complex band structure and band structure (black line) at different slice positions. (a) y=1 mm, (b) y=3 mm, (c) y=5 mm, (d) y=7 mm, (e) y=9 mm, (f) y=10 mm.

VI. CONCLUSION

We studied the propagation of Lamb waves under the condition of one-dimensional periodicity of the metastrip and the viscoelastic behavior is studied by comparing two materials: steel and epoxy. Based on the finite element method, we calculate the complex band structure and transmission spectrum of the two-dimensional metastrip, and its transmission spectrum was measured experimentally. The K-V model is added to the calculation of the complex band structure and transmission spectrum to make the numerical results more accurate. The exponential decay curve obtained from the numerical results coincides with the experimental results, which characterizes the decay of the evanescent wave numerically and experimentally by using the complex band structure and we successfully used complex band structure to predict simulation displacement distribution curve. Finally, we investigated the effects of different slicing forms on the complex band structure and transmission spectrum, and showed that different slicing forms can change the complex band structure. I-type slicing form leads to the ap-

pearance of deaf bands, which in turn do not get excited. Different slice forms affect the complex band structure. It causes the frequency to change between the different modes and opens the band gap and a rejection band appears.

VII. ACKNOWLEDGMENTS

Financial support from the National Natural Science Foundation of China (12122207 and 12021002) is gratefully acknowledged. Y.-F.W. acknowledges support from the Natural Science Foundation of Tianjin (20JCQNJC01030). V.L. acknowledges support from the EIPHI Graduate School (ANR-17-EURE-0002).

Appendix A: Evanescent wave propagation in metastrip made of steel

The selection of material parameters in simulation is based on experiment. In this work, the material parameters of the steel are Young's modulus $E = 210$ Gpa, Poisson's ratio $\nu = 0.3$ and mass density $\rho = 7850$ kg/m^3. The complex band structure of the H-type unit cell of steel and the transmission of the metastrip is calculated, as shown in Fig. 7.

It is obviously found that there are three band gaps in the range of 20.2-23.4 kHz, 27.6-46.5 kHz and 53.8-64.5 kHz, and they are shaded in the Fig. 8(a). In Fig. 8(b), the blue line is the result of the experiment and the red line represents result of the simulation. We use the transmission spectrum to verify the complex band structure. Compared with the results between the experiment and the simulation, the experimental curve is consistent with the simulation curve. In the band gap, the reduction of the transmission can be clearly observed.

In order to further study the wave attenuation characteristics, we select the frequency at 35 kHz and 60 kHz from the real part of Fig. 8(a) in the band gap, and the results are shown in Fig. 9. It can be observed that the plate wave has an attenuation effect inside the band gap. At 35 kHz, the waves are separated through about one unit cells, while at 60 kHz the waves are separated through about three unit cells. The experiment can get similar results to the simulation. According to the imaginary part of the complex band structure it can be observed that at the frequency of 60 kHz, the minimum imaginary part is small compared to that of 35 kHz, so the decay of the evanescent wave is slower and therefore the evanescent wave can pass through more unit cell structures, while at 35 kHz it can only pass through the first cells.

The images of the displacement according to the change of coordinates are given. The imaginary part has a parabolic variation and has a maximum at the central frequency as shown in Fig. 8(a). We select two frequency points (35kHz and 60kHz) and plot the displacement distribution curves at the top surface of the structure, as shown in Fig. 9. Same as epoxy, we use the modes of the complex band structure to predict the curves obtained from the simulation. The red lines in Figs. 9. (a) and (b) represent the displacement distribution curve obtained from simulation and experiment at 35 kHz. The green dashed line represent the predicted curve by using complex structure.The modes of the complex band structure are found at the corresponding frequencies and their displacement fields are extracted and multiplied by the coefficients of decay, and finally their prediction curves are obtained. The blue dashed line indicates the displacement distribution curve. Similarly, Fig. 9(c) and (d) represent the displacement distribution curve for simulation and experiment at 60 kHz, respectively. The simulated numerical curves largely coincide with the predicted curves and the feasibility of fitting the numerical curve using the modes of the complex band structure is demonstrated. For the attenuation curves at different frequencies, the attenuation trends are different. This is related to the degree of attenuation of the evanescent wave, the minimum imaginary value of the complex band structure.

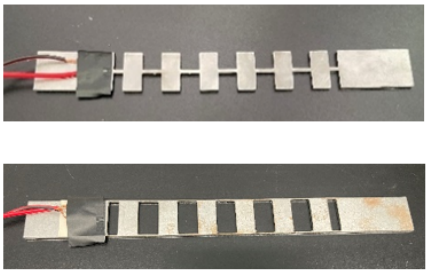

Figure 7: The metastrip of steel. The top metastrip is H-type and the bottom metastrip is I-type.

Similarly, we calculated the complex band structure as well as the transmission spectrum for the I-type steel metastrip, and the results are shown in Fig. 10. The complex band structure of the steel material is similar to that of the epoxy material. The deaf band can be observed at point A and the in-plane mode at point B and the same oscillation phenomenon appears in the transmission spectrum. Here, we can still use the elastic model to get a better transmission spectrum.

* Electronic address: wangyanfeng@tju.edu.cn

[1] M. S. Kushwaha, P. Halevi, L. Dobrzynski, and B. Djafari-

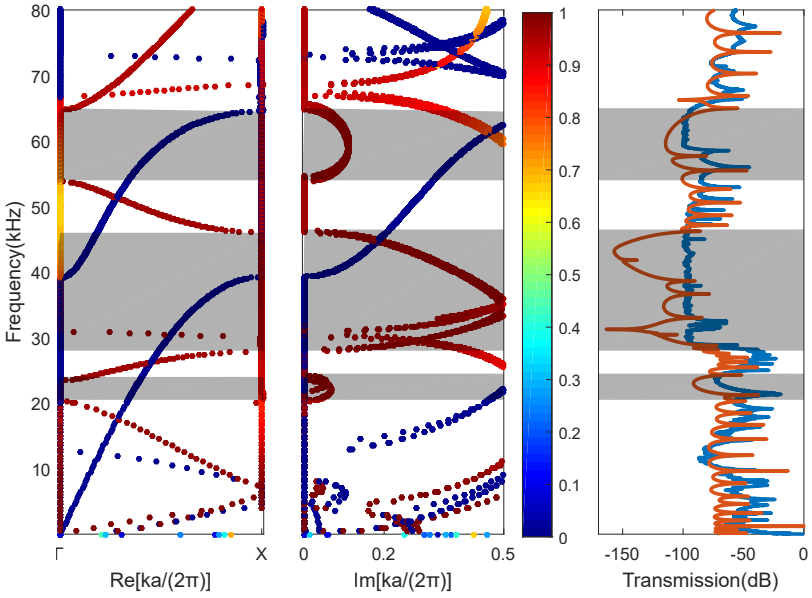

(a) (b)

Figure 8: Complex band structure (a) and transmission spectrum (b) of the steel metastrip. The left and right panels in (a) show the variation of frequency with the real and imaginary wave numbers respectively. The colorscale indicates the polarization of waves from in-plane modes (blue) to out-of-plane mode (red). The grey area represents the band gap. Regarding the transmission spectrum, the red line represents the numerical result. The blue lines represent the experimental result.

Rouhani, Physical review letters **71**, 2022 (1993).

[2] Y. Tanaka and S.-i. Tamura, Physical Review B **58**, 7958 (1998).

[3] Q. Yang, T. Song, X.-D. Wen, H.-F. Zhu, Z.-H. Tan, L.-J. Liu, Z.-J. Liu, and X.-W. Sun, Physics Letters A **384**, 126885 (2020).

[4] Y. Zhang, W. Feng, and W. Che, in *2016 IEEE International Conference on Microwave and Millimeter Wave Technology (ICMMT)* (IEEE, 2016), vol. 1, pp. 380–382.

[5] S. Mukherjee and E. H. Lee, Computers & Structures **5**, 279 (1975).

[6] R. Sprik and G. H. Wegdam, Solid State Communications **106**, 77 (1998).

[7] V. Laude, Y. Achaoui, S. Benchabane, and A. Khelif, Physical Review B **80**, 092301 (2009).

[8] X. Ao and C. T. Chan, Physical Review B **80**, 235118 (2009).

[9] Y.-F. Wang, S.-Y. Zhang, Y.-S. Wang, and V. Laude, Physical Review B **102**, 144303 (2020).

[10] L. Han, Y. Zhang, Z.-Q. Ni, Z.-M. Zhang, and L.-H. Jiang, Physica B: Condensed Matter **407**, 4579 (2012).

[11] L. Liu and M. I. Hussein, Journal of Applied Mechanics **79** (2012).

[12] L. Airoldi and M. Ruzzene, New Journal of Physics **13**, 113010 (2011).

[13] M. Oudich and M. Badreddine Assouar, Journal of Applied Physics **112**, 104509 (2012).

[14] N. Gao, B. Wang, K. Lu, and H. Hou, Applied Acoustics **177** (2021).

[15] J. D. Ferry, *Viscoelastic properties of polymers* (John Wiley & Sons, 1980).

[16] J. Li, P. Yang, Q. Ma, and M. Xia, Acta Mechanica **232**, 2933 (2021).

[17] J. Yi, Z. Li, M. Negahban, R. Xia, and J. Zhu, Mechanical Systems and Signal Processing **162**, 108101 (2022).

[18] M. Lewińska, V. Kouznetsova, J. Van Dommelen, A. Krushynska, and M. Geers, International Journal of Solids and Structures **126**, 163 (2017).

[19] M. Collet, M. Ouisse, M. Ruzzene, and M. Ichchou, International Journal of Solids and Structures **48**, 2837 (2011).

[20] A. Krushynska, V. Kouznetsova, and M. Geers, Journal of the Mechanics and Physics of Solids **96**, 29 (2016).

[21] J. Lou, L. He, J. Yang, S. Kitipornchai, and H. Wu, Applied Acoustics **141**, 382 (2018).

[22] A. O. Krushynska, A. S. Gliozzi, A. Fina, D. Krushinsky, D. Battegazzore, M. A. Badillo-Ávila, M. Acuautla, S. Stassi, C. Noè, N. M. Pugno, et al., Advanced Functional Materials **31**, 2103424 (2021).

[23] A. Palermo and A. Marzani, International Journal of Solids and Structures **191**, 601 (2020).

[24] T.-T. Wang, Y.-F. Wang, Y.-S. Wang, and V. Laude, Applied Physics Letters **111**, 041906 (2017).

[25] V. Romero-García, J. V. Sánchez-Pérez, S. Castiñeira-Ibáñez, and L. Garcia-Raffi, Applied Physics Letters **96**, 124102 (2010).

[26] V. Romero-García, J. V. Sánchez-Pérez, and L. M. Garcia-Raffi, Journal of Applied Physics **108**, 044907 (2010).

[27] V. Romero-García, L. M. Garcia-Raffi, and J. V. Sánchez-Pérez, Aip Advances **1**, 041601 (2011).

[28] Y. F. Wang, T. T. Wang, J. W. Liang, Y. S. Wang, and L. Vincent, Journal of Sound and Vibration **437**, S0022460X18306151 (2018).

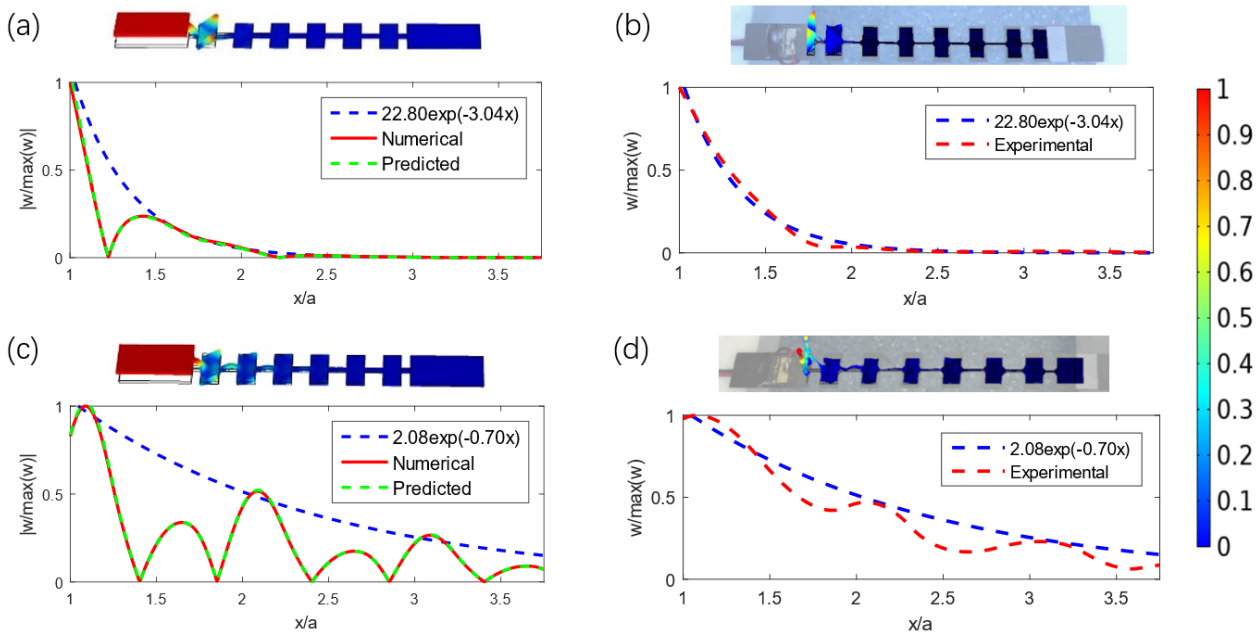

Figure 9: Attenuation of evanescent waves in metastrip. Panels (a) and (b) show the displacement distribution of the metastrip at 35 kHz obtained from simulations and experiment, respectively. The colorscale represents the amplitude of normalized displacement. Numerical displacement distribution along the central line of the top surface is shown in solid line in the bottom part of panel (a). Measured displacement distribution along the central line of the top surface is shown in solid line in the bottom part of panel (b). The predicted results are shown by green dashed lines where $\alpha = 0.5$, $k_1 = -3.02 + 9.42i$, $\beta = 0.5$, $k_2 = -3.01 + 3.14i$. The bule dashed line represents the exponential-like decay of the measured displacement fitted by the minimu imaginary part of the wave number in the complex band structure. Panels (c) and (d) show the similar results at 60 kHz. Where the coefficients in the prediction curve $\alpha = 0.5$, $k_1 = -0.66$, $\beta = 0.5$, $k_2 = -0.66 + 6.28i$.

[29] F.-C. Hsu, C.-I. Lee, J.-C. Hsu, T.-C. Huang, C.-H. Wang, and P. Chang, Applied Physics Letters **96**, 051902 (2010).
[30] T.-T. Wu and Z.-G. Huang, Physical Review B **70**, 214304 (2004).

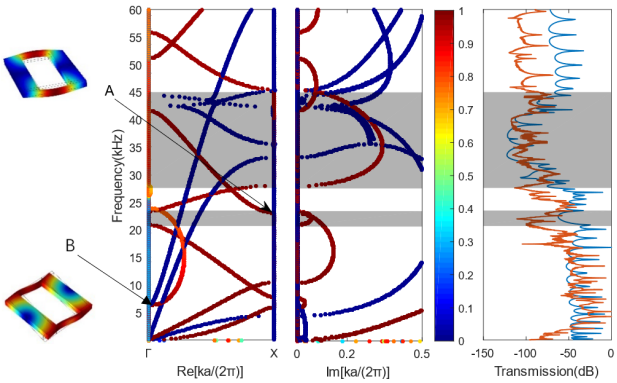

Figure 10: The complex band structure and transmission spectrum for the steel metastrip. (a) The complex band structure for the I-type steel metastrip and the modal distributions at marked points A and B. The left and right plots show the frequency variation with the real and imaginary wave number, respectively. The grey regions represent the band gaps. Panel (b) shows the transmission spectrum. The blue and red lines represent the experimental and simulated results, respectively.